Analysis of the competition between forbidden and hyperfine-induced transitions in Ne-like ions

Martin Andersson,[1,2,3] Jon Grumer,[1,*] Tomas Brage,[1] Yaming Zou,[2,3] and Roger Hutton[2,3,†]
[1]*Division of Mathematical Physics, Department of Physics, Lund University, SE-221 00 Lund, Sweden*
[2]*The Key Laboratory of Applied Ion Beam Physics, Ministry of Education, People's Republic of China*
[3]*Shanghai EBIT Laboratory, Institute of Modern Physics, Fudan University, Shanghai 200433, People's Republic of China*
(Received 2 November 2015; published 14 March 2016)

In this work we investigate the decay of the $|2p^5\,3s\ ^3P_0\rangle$ state in neon-like ions along the isoelectronic sequence ranging from $Z = 10$ to $Z = 35$. In the absence of a nuclear spin, the magnetic dipole transition to $|2p^5\,3s\ ^3P_1\rangle$ is the dominating decay channel. However, for isotopes with a nuclear spin, the interaction between the nuclear magnetic dipole moment and the electronic field introduces a mixing of $|2p^5\,3s\ ^3P_1\rangle$ and $|\,^1P_1\rangle$ into the $|\,^3P_0\rangle$ state, which in turn opens up a competing hyperfine-induced electric dipole decay channel to the ground state. This hyperfine-induced transition channel clearly dominates over the magnetic dipole channel for the neutral end of the isoelectronic sequence, when present. We give values for the rates of both these competing channels and discuss how the introduction of the hyperfine-induced transition channel could have a dramatic influence on the spectrum, not only because it introduces a new line, but also since it can substantially decrease the intensity of the magnetic dipole $2p^5\,3s\ ^3P_0 \rightarrow 2p^5\,3s\ ^3P_1$ line and affect the predicted ionization balance in different plasmas.

DOI: 10.1103/PhysRevA.93.032506

I. INTRODUCTION

Lines from the $2p^5\,3l \rightarrow 2p^6$ transitions in Ne-like ions are prominent in the x-ray spectra of many laser-produced [1,2], Tokamak [3], solar coronal [4], and stellar [5] plasmas. Ne-like ions are therefore of great importance for plasma diagnostics and have attracted both theoretical and experimental attention. On the theoretical side a wide range of calculations has been performed for excitation energies and transition rates, using methods based on, e.g., the Z-expansion technique [6], model potential approach [7], configuration nteraction (CI) method [8], multiconfiguration Hartree-Fock (MCHF) method [9], Dirac-based relativistic many-body perturbation theory (RMBPT) [10,11], and relativistic multireference many-body Möller-Plesset (MR-MP) perturbation theory [12] and a combination of the configuration interaction method and many-body perturbation theory (CI-MBPT) [13]. Recently Li *et al.* [14] presented results on the angular dependence of the $^3P_2 \rightarrow\ ^1S_0$ transition for Ne-like ions in general and for Mg II in more detail.

The photoionization of Ne-like ions has also been studied theoretically, e.g., by using the R-matrix method, both in the nonrelativistic [15] and in the relativistic [16] version. There are also results for excitation cross sections from, e.g., nonrelativistic [17] and Dirac-based [18] distorted-wave approaches, as well as the Breit-Pauli R-matrix [19] and Dirac R matrix [20,21] methods.

On the experimental side, Ne-like ions have been investigated, e.g., by Westerlind *et al.* [22] using beam-foil spectroscopy, Kaufman *et al.* [23] using a spark source, Gordon *et al.* [24] and Jupén *et al.* [25] using laser-produced plasmas, Beiersdorfer *et al.* [26] and Gu *et al.* [27] using electron beam ion traps, and Beiersdorfer *et al.* [3] using a Tokamak plasma.

It is a common assumption that predictions of the rates of forbidden transitions are a challenge to atomic theory. However, this is certainly not always the case, since it is important to distinguish between *expected* and *unexpected* transitions as defined by Brage *et al.* [98] (see [47] for a review of unexpected transitions). According to this, an expected transition is insensitive to the mixing between states represented in the "best" coupling scheme, for example, LS coupling, whereas unexpected transitions only occur due to deviations from this coupling scheme, i.e., due to mixing between states. One example of an unexpected transition in neon-like ions is the spin-forbidden electric dipole transition $2p^5\,3s\ ^3P_1 \rightarrow 2p^6\ ^1S_0$. This transition is induced through relativistic effects which give a small mixing between the $|2p^5\,3s\,^3P_1\rangle$ and the $|2p^5\,3s\ ^1P_1\rangle$ states, opening up this new $E1$ decay channel.

This paper focuses on the decay of the metastable $2p^5\,3s\,^3P_0$. The structure of neon-like ions is illustrated in Fig. 1, for nuclear charge $Z \leqslant 35$, showing possible decay channels of the different $2p^5\,3s$ states. We limit our discussion to this range of ions, since for $Z \geqslant 36$ the $2p^5\,3p\,^3S_1$ level is lower in energy than at least some of the $2p^5 3s$ levels, which opens up a new electric dipole ($E1$) decay from the $^3P_0$. For this low-Z end of the isoelectronic sequence, and for isotopes without nuclear spin, the dominant decay channel for the $2p^5\,3s\,^3P_0$ level is the magnetic dipole ($M1$) transition to $^3P_1$. The electric quadrupole ($E2$) transition to the $^3P_2$ level has a rate that is between 3 and 4 orders of magnitude smaller. However, for isotopes with a nonzero nuclear spin, the hyperfine interaction introduces a mixing of the $2p^5\,3s\,^3P_0$ level with $2p^5\,3s\,^3P_1$ and $^1P_1$ opening a *hyperfine-induced electric dipole transition* (HIT) to the ground state. In this paper we discuss the competition between these decay channels and report on critically evaluated theoretical calculations to represent this system.

One of the new results we present is the fact that the hyperfine-induced transition (HIT) channel clearly dominates over the magnetic dipole channel for ions at the neutral end of the isoelectronic sequence, with up to four orders of magnitude. The magnetic dipole transition increases more rapidly with Z than the HIT and will gradually, with increasing nuclear charge, dominate as the fastest decay from $^3P_0$.

*jon.grumer@teorfys.lu.se
†rhutton@fudan.edu.cn

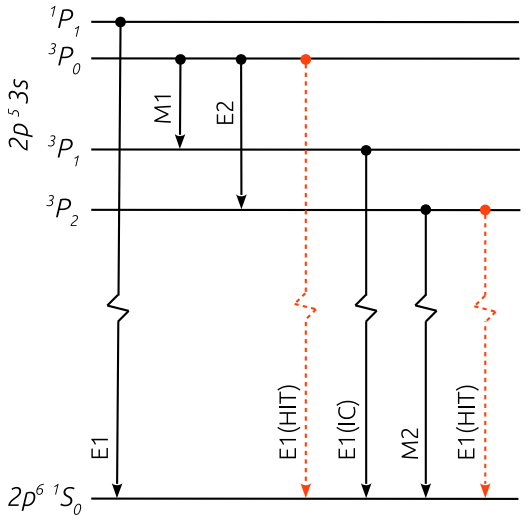

FIG. 1. Schematic energy level diagram of the ground $2p^6\ ^1S_0$ and first excited $2s^5\,3s\ ^{1,3}P$ levels of Ne-like ions. Included transitions are labeled by their multipolarity ($E1$, $M1$, $E2$, and $M2$). Some decay channels are also labeled HIT, implying a *hyperfine-induced transition* (these lines are dashed, as they only appears for isotopes with a nuclear spin), or IC, referring to an *intercombination*, i.e., spin-induced, transition.

However, the HIT could still be important in cases of isotopes with large nuclear magnetic dipole moments.

Clearly the introduction of a hyperfine-induced transition channel from $2p^5\,3s\ ^3P_0$ to the ground state will have a dramatic influence on the spectrum of the Ne-like ions, not only because it introduces the new $2p^5\,3s\ ^3P_0 \rightarrow 2p^6\ ^1S_0$ line, but also since it can substantially decrease the intensity of the magnetic dipole $2p^5\,3s\ ^3P_0 \rightarrow 2p^5\,3s\ ^3P_1$ line. In addition, we should expect changes in the predicted charge state balance in many plasmas, if the lifetime of the $^3P_0$ is changed. It is intriguing to conclude that this will even be an isotope-dependent effect, since the HIT depends on the nuclear spin.

A. Investigations of hyperfine-induced transitions

Since the mid 1990s there has been a range of theoretical investigations of HITs from the first excited $ns\,np\ ^3P_0$ level in Be-like ($n = 2$) [28–31], Mg-like ($n = 3$) [29,32,33], and Zn-like ($n = 4$) [34] systems. In these ions, for isotopes with a nuclear spin, there will be a HIT, which in general dramatically shortens the lifetime of the $^3P_0$ level.

On the experimental side, Brage *et al.* [35] used observations of the planetary nebula NGC3918 to determine the hyperfine-induced decay rate of $2s\,2p\ ^3P_0$ for an admixture of Be-like $^{14}N^{3+}$ and $^{15}N^{3+}$. Schippers *et al.* [36,37] measured the lifetime of the same level in $^{47}Ti^{18+}$ and $^{33}S^{+12}$, while Rosenband *et al.* determined the lifetime of $3s\,3p\ ^3P_0$ in magnesium-like $^{27}Al^+$ [38].

The case discussed in this paper is somewhat different, since the HIT is competing with another single-photon channel: the $M1$ decay to $^3P_1$. We have reported earlier on a similar situation in nickel-like ions [39–43] where the first excited state $3d^9\,4s\ ^3D_3$ can decay through both an $M3$ and a hyperfine-induced $E2$ transition to the ground states $3d^{10}$. Träbert *et al.* [44] performed lifetime measurements for this level in isotope-pure Ni-like ^{129}Xe and ^{132}Xe, confirming our theoretical predictions. Another example is the third excited $ns\,np\ ^3P_2$ level in Be-like and Zn-like systems, which can decay through both an $M2$ and a hyperfine-induced E1 to the ground states $ns^2\ ^1S_0$ [31,33]. In connection with the goal of designing ultraprecise optical clocks, Porsev and Derevianko [45] performed calculations investigating how the hyperfine interaction influences the lifetime of the first $^3P_2$ level in neutral Mg, Ca, Sr, and Yt. Chen and Cheng [46] revisited how the lifetime of $4s\,4p\ ^3P_2$ is affected by hyperfine interaction along the Zn-like isoelectronic sequence. An overview of unexpected transitions [hyperfine-, spin (intercombination)-, and magnetic-field-induced transitions] is given by Grumer *et al.* [47]. A comprehensive review of hyperfine-dependent lifetimes was published by Johnson [48].

Returning to Ne-like systems, Beiersdorfer *et al.* [49] reported on calculations for the decay of the $2p^5\,3s\ ^3P_0$ level using the Flexible Atomic Code (FAC) [50], which employs a relativistic CI method combined with RMBPT. The aim of their work was to investigate which ions would be suitable for lifetime measurements of the level. However, since the hyperfine-induced transition channel was not included, we show that their conclusions have to be revised.

II. THEORY

A. Hyperfine interaction

When the nucleus has a spin $\boldsymbol{I}$, there is an interaction between its electromagnetic multipole moments and the electrons. This interaction couples the total electronic angular momentum $\boldsymbol{J}$ and the nuclear spin $\boldsymbol{I}$ to a new total angular momentum $\boldsymbol{F}$ and each fine-structure level is split up into multiple hyperfine levels. Since the hyperfine interaction operator $\mathcal{H}_{\rm hpf}$ does not commute with the $\boldsymbol{J}^2$ operator, a mixing between states with different J quantum numbers is introduced, which in turn might open up new, unexpected transition channels.

In this report we are interested in the mixing of the $|2p^5\,3s\ ^3P_1\rangle$ and the $|\,^1P_1\rangle$ states with the $|\,^3P_0\rangle$ state. Since we are focusing on levels with $J = 0$, only the nuclear magnetic dipole hyperfine interaction can give rise to the mixing, and higher orders of hyperfine interaction are therefore omitted. We can then express the interaction as

$$\mathcal{H}_{\rm hpf} = \boldsymbol{T}^{(1)} \cdot \boldsymbol{M}^{(1)}, \tag{1}$$

where $\boldsymbol{T}^{(1)}$ and $\boldsymbol{M}^{(1)}$ are spherical tensors of rank 1. The former operates on the electronic part of the wave function, and the latter on the nuclear part. The hyperfine interaction matrix element between two hyperfine states, $|\gamma I J F M_F\rangle$ and $|\gamma' I J' F M_F\rangle$, can be expressed as

$$\begin{aligned} W(JF,J'F) &= \langle \gamma I J F M_F | \mathcal{H}_{\rm hpf} | \gamma' I J' F M_F \rangle \\ &= (-1)^{I+J+F} \sqrt{(2J+1)(2I+1)} \begin{Bmatrix} I & J & F \\ J' & I & 1 \end{Bmatrix} \\ &\quad \times \langle \gamma J || \boldsymbol{T}^{(1)} || \gamma' J' \rangle \langle I || \boldsymbol{M}^{(1)} || I \rangle, \end{aligned}$$

where we use the Brink and Satchler definition of the reduced matrix element [51]. For the nuclear part, we use the

convention of defining the nuclear magnetic dipole moment, μ_I,

$$\langle I||\boldsymbol{M}^{(1)}||I\rangle = \mu_I\sqrt{\frac{I+1}{I}}. \tag{2}$$

Values of μ_I are tabulated in, e.g., Stone's compilation [52]. The matrix elements can then be expressed as

$$\begin{aligned} &W(JF,(J-1)F) \\ &\quad= (-1)^{(I+J+F)}\mu_I\sqrt{\frac{(2I+1)(I+1)(2J+1)}{I}} \\ &\qquad\times\begin{Bmatrix} I & J & F \\ J-1 & I & 1 \end{Bmatrix}\langle\gamma J||\mathbf{T}^{(1)}||\gamma'(J-1)\rangle, \end{aligned}$$

which can be further simplified (see, for example, Sobelman [53]) to the expression

$$\begin{aligned} &W(JF,(J-1)F) \\ &\quad= \left[\frac{(K-2J+1)(K+1)(K-2F)(K-2I)}{J(2J-1)}\right]^{1/2} \\ &\qquad\times\frac{\mu_I}{2I}\langle\gamma J||\mathbf{T}^{(1)}||\gamma'(J-1)\rangle, \end{aligned} \tag{3}$$

where

$$K = F + J + I. \tag{4}$$

We define the off-diagonal hyperfine constant $A(J,J-1)$ as

$$A(J,J-1) = \mu_I\frac{1}{I\sqrt{J(2J-1)}}\langle\gamma J||\mathbf{T}^{(1)}||\gamma'(J-1)\rangle, \tag{5}$$

and using Eq. (3) the interaction can be rewritten as

$$\begin{aligned} &W(JF,(J-1)F) \\ &\quad= \frac{A(J,J-1)}{2}\sqrt{[J^2-(I-F)^2][(I+F+1)^2-J^2]}. \end{aligned} \tag{6}$$

From this expression, and using that in the present case $F = I$, it is straightforward to show that

$$W\left({}^xP_1F,\,{}^3P_0F\right) = \sqrt{I(I+1)}A\left({}^xP_1,\,{}^3P_0\right), \tag{7}$$

where x refers to the singlet or the triplet case.

B. Transitions between hyperfine levels

The transition probability for an electric dipole transition between two hyperfine levels is given by

$$\begin{aligned} &\mathcal{A}_{E1}(\gamma IJF,\gamma' IJ'F') \\ &\quad= \frac{(2\pi)^3}{3\hbar\lambda^3}\frac{1}{2F'+1}|\langle\gamma IJF||D^{(1)}||\gamma' IJ'F'\rangle|^2. \end{aligned} \tag{8}$$

The reduced matrix elements can in turn be expressed in terms of J-dependent reduced matrix elements as

$$\begin{aligned} &\langle\gamma IJF||D^{(1)}||\gamma' IJ'F'\rangle \\ &\quad= (-1)^{J+I+F'+1}\sqrt{(2F+1)(2F'+1)} \\ &\qquad\times\begin{Bmatrix} J & I & F \\ F' & 1 & J' \end{Bmatrix}\langle\gamma J||D^{(1)}||\gamma' J'\rangle. \end{aligned} \tag{9}$$

In this work we are interested in transitions to the lower state with $J = 0$ ($2p^6\,{}^1S_0$), which has only one hyperfine level with $F = I$. Applying orthogonality relations for the 6-j symbols gives

$$\mathcal{A}_{E1}(\gamma IJF,\gamma' IJ'F') = \frac{(2\pi)^3}{3\hbar\lambda^3}\frac{1}{2J'+1}|\langle\gamma J||D^{(1)}||\gamma' J'\rangle|^2, \tag{10}$$

i.e., the same expression as for the transition between the fine-structure levels in the case of an isotope with zero nuclear spin.

C. Hyperfine mixing of $2p^5\,3s\,{}^3P_0$

The hyperfine mixing of $|2p^5\,3s\,{}^3P_1\rangle$ and $|\,{}^1P_1\rangle$ with $|\,{}^3P_0\rangle$ opens up an unexpected electric dipole transition from the latter to the ground state $|2p^6\,{}^1S_0\rangle$. The rate of this transition can be expressed as

$$\begin{aligned} &\mathcal{A}_{\rm HIT}\left({}^1S_0(F=I),\ {}^3P_0(F=I)\right) \\ &\quad= \frac{(2\pi)^3}{9\hbar\lambda^3}\left|{}^{c1}P_1(F)\left\langle{}^1S_0\left||D^{(1)}|\right|{}^1P_1\right\rangle\right. \\ &\qquad\left.+{}^{c3}P_1(F)\left\langle{}^1S_0\left||D^{(1)}|\right|{}^3P_1\right\rangle\right|^2, \end{aligned} \tag{11}$$

where ${}^{c1}P_1$ and ${}^{c3}P_1$ are mixing coefficients with $|\,{}^1P_1\rangle$ and $|\,{}^3P_1\rangle$, respectively. The mixing coefficients are determined from first-order perturbation theory,

$${}^{cx}P_1(F) = \frac{\langle I^xP_1FM_F|\mathcal{H}_{\rm hpf}|I\,{}^3P_0\,FM_F\rangle}{E\left({}^3P_0\right)-E\left({}^xP_1\right)}, \tag{12}$$

where the x superscript refers to the singlet or triplet state. Using Eq. (7), we get

$${}^{cx}P_1(F) = \frac{\sqrt{I(I+1)}A\left({}^xP_1,\,{}^3P_0\right)}{E\left({}^3P_0\right)-E\left({}^xP_1\right)}. \tag{13}$$

The hyperfine-induced transition rate to the ground state can then be expressed as (with $F = I$)

$$\begin{aligned} &\mathcal{A}_{\rm HIT}\left({}^1S_0\,F,\ {}^3P_0\,F\right) \\ &\quad= \frac{(2\pi)^3}{9\hbar\lambda^3}I(I+1)\left|\frac{A\left({}^1P_1\,,\,{}^3P_0\right)}{E\left({}^3P_0\right)-E\left({}^1P_1\right)}\left\langle{}^1S_0\left||D^{(1)}|\right|{}^1P_1\right\rangle\right. \\ &\qquad\left.+\frac{A\left({}^3P_1\,,\,{}^3P_0\right)}{E\left({}^3P_0\right)-E\left({}^3P_1\right)}\left\langle{}^1S_0\left||D^{(1)}|\right|{}^3P_1\right\rangle\right|^2. \end{aligned} \tag{14}$$

Using Eq. (5) one can define an off-diagonal hyperfine interaction matrix element which depends only on the electronic part of the wave function,

$$A^{\rm elec}(J,J-1) = \frac{I}{\mu_I}A(J,J-1), \tag{15}$$

which makes it easier to investigate trends along the isoelectronic sequence. Using this and eliminating the explicit I dependence in Eq. (14) we can express the electronic

hyperfine-induced electric dipole transition as

$$\mathcal{A}^{\rm elec}_{\rm HIT}\left({}^1S_0\,,\ {}^3P_0\right) = \frac{I}{\mu_I^2(I+1)}\mathcal{A}_{\rm HIT}\left({}^1S_0\,,\ {}^3P_0\right) = \frac{(2\pi)^3}{9\hbar\lambda^3}\left|\frac{A^{\rm elec}\left({}^1P_1\,,\ {}^3P_0\right)}{E({}^3P_0)-E({}^1P_1)}\left\langle {}^1S_0\left|\left|D^{(1)}\right|\right|{}^1P_1\right\rangle + \frac{A^{\rm elec}\left({}^3P_1\,,\ {}^3P_0\right)}{E\left({}^3P_0\right)-E\left({}^3P_1\right)}\left\langle {}^1S_0\left|\left|D^{(1)}\right|\right|{}^3P_1\right\rangle\right|^2. \tag{16}$$

Since this rate depends only on the electronic part of the wave function, it is expected to vary smoothly along the isoelectronic sequence.

III. THE MULTICONFIGURATION DIRAC-HARTREE-FOCK (MCDHF) METHOD

The calculations in this work are based on the MCDHF method [54], using the GRASP2K program suite [55,56]. The MCDHF method is founded on the assumption that the atomic-state function (ASF), $|\Gamma J M_J\rangle$, can be described as a linear combination of configuration-state functions (CSFs), $|\gamma_i J M_J\rangle$,

$$|\Gamma J M_J\rangle = \sum_i c_i |\gamma_i J M_J\rangle. \tag{17}$$

In turn, the CSFs are represented by a sum, according to spin-angular coupling rules, of products of one-electron Dirac orbitals of the form

$$\phi(r,\theta,\varphi,\sigma) = \frac{1}{r}\begin{pmatrix} P(r)\chi_{\kappa m}(\theta,\varphi,\sigma) \\ i\,Q(r)\chi_{-\kappa m}(\theta,\varphi,\sigma)\end{pmatrix}, \tag{18}$$

where the angular- and spin-dependent parts are assumed to be known, but the radial parts, $P(r)$ and $Q(r)$, are determined from variational calculations.

We start from the Dirac-Coulomb Hamiltonian

$$H_{\rm DC} = \sum_i (c\alpha_i \cdot p_i + (\beta_i - 1)c^2 + V_i) + \sum_{i>j}\frac{1}{r_{ij}}, \tag{19}$$

where V_i is the monopole part of the electron-nucleus Coulomb interaction, Z/r_i, corrected for a finite nucleus, and optimize the ASF in a self-consistent field procedure where both the radial part of the Dirac orbitals and the expansion coefficients c_i are optimized to self-consistency. In a subsequent CI calculation [57] the Breit interaction in the low-frequency limit and QED effects are included.

After we have obtained the ASFs we can compute properties such as the transition probabilities and hyperfine interaction constants. The transition matrix elements can be expressed in the Babushkin or Coulomb gauge [58], which allows for accuracy studies of the applied model. Since ASFs of different parities, in general, are built from independently optimized sets of Dirac orbitals, they are not restricted to be orthonormal, and a biorthogonal transformation technique [59] is applied to be able to evaluate the transition properties using standard Racah algebra. The reduced hyperfine interaction matrix elements are determined from the obtained ASFs via the GRASP2K module HFSZEEMAN [60].

IV. ELECTRON CORRELATION MODEL

Our calculations are based on the restricted active space method [61–63]. The restricted-active-space method is an "orbital-driven" technique where the calculations are enlarged in a systematic manner to enable us to study the convergence of our results for important properties. In this way, we systematically investigate different contributions to the correlation. From this it is clear that it is important to include both valance-valence and core-valance correlations with the $2s$ subshell [64] (we treat the $2p$ subshell as part of the valence electrons).

The calculations start by defining a multireference set of configurations. From this we allow single and double substitutions to a systematically increasing active set of orbitals. It is customary to include the complex of the states of interest in the multireference set, i.e., all configurations with the same set of principle quantum numbers and parity [65]. The complex of the ground state, $2s^2\,2p^6$, includes only one state, whereas the complex of the excited states of interest here consists of $\{2s^2\,2p^5\,3s,\ 2s^2\,2p^5\,3d,\ 2s\,2p^6\,3p\}$. However, we found that the inclusion of the $2s\,2p^6\,3p$, with an open $2s$ subshell, has only a very small effect on the results, while increasing the size of our calculations substantially. It was therefore left out of the final multireference set.

In the first step of our calculations we use only the multireference set of configurations in our expansions, The spin orbitals are optimized in an extended-optimal-level calculation [66]. For the following steps, the goal is to include valence-valence and core-valence interaction with the $2s$ subshell to convergence. We therefore restrict the single and double excitations from the multireference set to include only configurations of the form

$$1s^2 2s^2 2p^4 n_1 l_1 n_2 l_2, \quad 1s^2 2s 2p^5 n_1 l_1 n_2 l_2$$

for the ground state and

$$\begin{array}{ll} 1s^2 2s^2 2p^4 n_1 l_1 n_2 l_2, & 1s^2 2s^2 2p^3 3s n_1 l_1 n_2 l_2, \\ 1s^2 2s 2p^5 n_1 l_1 n_2 l_2, & 1s^2 2s 2p^4 3s n_1 l_1 n_2 l_2, \\ 1s^2 2s^2 2p^3 3d n_1 l_1 n_2 l_2, & 1s^2 2s 2p^4 3d n_1 l_1 n_2 l_2 \end{array}$$

for the excited state.

The restricted active space is enlarged in a systematic way, by stepwise increasing the maximum n quantum number of the active set of orbitals [63]. In each step only the new orbitals were optimized in the extended-optimal-level scheme for the states of interest. The active sets are labeled according to

$$\begin{aligned} n3 &= \{2s,2p,3s,3p,3d\}, \\ n4 &= n3 + \{4s,4p,4d,4f\}, \\ n5 &= n4 + \{5s,5p,5d,5f,5g\}, \\ n6 &= n5 + \{6s,6p,6d,6f,6g\}. \end{aligned}$$

In the last step, to allow for spin polarization [67,68], an extended configuration set is used in a nonvariational, final CI calculation, without reoptimization of the orbitals. The configuration sets described above were then augmented by configurations of the types

$$\begin{array}{ll} 1s^1 2s^2 2p^5 n_1 l_1 n_2 l_2, & 1s^1 2s^1 2p^5 3s n_1 l_1 n_2 l_2, \\ 1s^1 2s^1 2p^5 3d n_1 l_1 n_2 l_2, & 1s^1 2s^2 2p^4 3s n_1 l_1 n_2 l_2, \\ 1s^1 2s^2 2p^4 3d n_1 l_1 n_2 l_2. & \end{array}$$

TABLE I. Excitation energy of the $2p^5 3s\ ^3P_1$ level and energies relative to this from our calculations and other theories and experiments. All energies in cm^{-1}. Energies followed by an asterisk are derived from interpolation or extrapolation (see text).

	$\Delta E\ (^3P_2)$		$E\ (^3P_1)$		$\Delta E\ (^3P_0)$		$\Delta E\ (^1P_1)$	
Ion	Our	Expt.	Our	Expt.	Our	Expt.	Our	Expt.
Ne	−410.30	−417.45[a]	1 34 070.65	1 34 459.29[a]	364.10	359.43[a]	1347.64	1429.43[a]
Na^+	−761.69	−765.30[b]	2 65 920.56	2 65 689.62[b]	592.78	592.00[b]	3025.46	3073.34[b]
Mg^{2+}	−1225.8	−1227.8[c]	4 27 337.3	4 26 868.1[c]	983.0	984.0[c]	4645.8	4661.9[c]
Al^{3+}	−1828.9	−1829.7[d]	6 19 046.0	6 18 473.9[d]	1583.6	1586.2[d]	6251.3	6243.6[d]
Si^{4+}	−2574.5	−2572.6[e]	8 41 204.6	8 40 590.0[e]	2475.3	2480.6[e]	7942.6	7921.2[e]
P^{5+}	−3450.9	−3445.4[f]	1 093 819.0	1 093 240.0[f]	3763.0	3772.1[f]	9854.4	9826.1[f]
S^{6+}	−4434	−4420[g]	1 376 845	1 376 218[g]	5574	5587[g]	12 149	12 127[g]
Cl^{7+}	−5492	−5468[h]	1 690 216	1689463[h]	8050	8059[h]	15 012	14 972[h]
Ar^{8+}	−6595	−6573[i]	2 033 858	2 033 118[i]	11 346	11 370[i]	18 629	18 610[i]
		−6637[lst]		2 033 140[lst]		11 372[lst]		18 610[lst]
K^{9+}	−7717	−7687[j]	2 407 702	2 406 855[j]	15 616	15 775[j]	23 187	23 282[j]
Ca^{10+}	−8841	−8820[k]	2 811 683	2 810 900[k]	21 019	21 195[k]	28 864	29 000[k]
		−8808[l]		2 810 850[l]		21 312[l]		29 126[l]
Sc^{11+}	−9957	−9929[m]	3 245 742	3 245 100[m]	27 717	27 630[m]	35 835	35 700[m]
Ti^{12+}	−11 060	−11 047[m]	3 709 828	3 709 200[m]	35 876	36 038[m]	44 273	44 400[m]
V^{13+}	−12 148	−12 094[m]	4 203 885	4 202 700[m]	45 668	45 710*[m]	54 353	54 400[m]
Cr^{14+}	−13 222	−13 206[m]	4 727 862	4 727 500[m]	57 277	56 674[m]	66 259	65 700[m]
Mn^{15+}	−14 282	−14 236[m]	5 281 704	5 281 200[m]	70 893	70 320*[m]	80 182	79 600[m]
Fe^{16+}	−15 330	−15 280[n]	5 865 359	5 864 770[n]	86 719	86 110*[o]	96 322	96 100[n]
		−15 270[p]		5 864 760[p]		86 718[p]		96 262[p]
Co^{17+}	−16 368		6 478 769	6 477 900[q]	1 04 968		1 14 893	1 14 500[q]
Ni^{18+}	−17 397	−17 340[r]	7 121 875	7 122 600[r]	1 25 864	1 25 100*[r]	1 36 116	1 35 500[r]
Cu^{19+}	−18 419	−18 380[r]	7 794 616	7 795 650[r]	1 49 643	1 48 300*[r]	1 60 228	1 59 400[r]
Zn^{20+}	−19 435		8 496 928	8 496 900[u]	1 76 555		1 87 475	1 86 700[u]
Ga^{21+}	−20 446		9 228 744	9 228 000[u]	2 06 859		2 18 117	2 20 000[u]
Ge^{22+}	−21 454	−20 000[s]	9 989 996	9 990 000[s]	2 40 829	2 40 000[s]	2 52 426	2 50 000[s]
As^{23+}	−22 459		10 780 609	10 789 000[u]	2 78 751		2 90 687	2 80 000[u]
Se^{24+}	−23 463		11 600 510	11 608 000[u]	3 20 924		3 33 199	3 34 000[u]
Br^{25+}	−24 466	−24 572[t]	12 449 619	12 453 300[t]	3 67 661	3 66 422[t]	3 80 272	3 78 569[t]

[a]From Saloman and Sansonetti [69].
[b]From Sansonetti [71].
[c]From Andersson and Johannesson [72].
[d]From Kaufman [23].
[e]From Brillet [75].
[f]From Eidelberg and Artru [77].
[g]From Jupén and Engström [79].
[h]From Jupén [81].
[i]From Engström and Berry [83].
[j]From Sansonetti [85].
[k]From Jupén *et al.* [87].
[l]From Ragozin *et al.* [70].
[m]From Jupén[25].
[n]From Buchet *et al.* [73].
[o]From Feldman *et al.* [74].
[p]From Zanna and Ishikawa [76].
[q]From Sugar and Corliss [78].
[r]From Buchet *et al.* [80].
[s]From Yuan *et al.* [82].
[t]From Jupén *et al.* [84].
[u]From NIST ASD [86].

V. RESULTS

In Table I we compare our calculated energies with experimental results. In this work, the most critical comparisons are for the excitation energies of the $2p^5 3s\ ^3P_0$ and the energy splitting between this level and $2p^5 3s\ ^3P_1$ and $^1P_1$, respectively [see Eq. (16)]. However, experimental excitation energies are, for obvious reasons, not known for all $^3P_0$ levels along the isoelectronic sequence. Therefore in the second

TABLE II. Lifetimes, τ, of the $2p^5 3s\ ^{1,3}P_1$ levels (in ps) for different ions in the Ne-like sequence from the present calculations compared to other theoretical results and from experiments.

	$\tau\ (^3P_1)$			$\tau\ (^1P_1)$		
Ion	Present theoretical	Other theoretical	Expt.	Present theoretical	Other theoretical	Expt.
Ne	21 468	22 730[a]	29 600 ± 1000[b]	1804	1609[a]	1470 ± 100[b]
			31 700 ± 1600[c]			1870 ± 180[c]
			29 800 ± 2000[d]			1300 ± 100[d]
Na^+	6580	6914[a]	6000 ± 1200[b]	318.2	301.8[a]	320^{+50}_{-40}[b]
		6130[e]	10 600 ± 500[f]		286[e]	580 ± 60[f]
Mg^{2+}	2031	2128[a]	1900 ± 190[g]	112.2	109.2[a]	100 ± 10[g]
		1870[e]			102[e]	110^{+15}_{-10}[b]
Al^{3+}	694.1	684.5[a]		52.56	51.58[a]	46^{+10}_{-5}[b]
		640[e]			48.5[e]	
Si^{4+}	265.5	260.7[a]		29.00	28.60[a]	28^{+8}_{-4}[b]
		244[e]			27.1[e]	
P^{5+}	113.4	116.7[a]	130 ± 30[b]	17.89	17.56[a]	18^{+7}_{-2}[b]
		106[e]			16.9[e]	
S^{6+}	53.74	55.07[a]	49.4 ± 0.2[h]	11.98	11.75[a]	11.9 ± 0.1[h]
		50.3[e]	52 ± 2[i]		11.4[e]	17.4 ± 0.5[i]
			48.7 ± 13.3[j]			12.0 ± 3.2[j]
Cl^{7+}	28.06	26.6[e]	27.1 ± 1[i]	8.536	8.16[e]	13 ± 1[i]
			34 ± 12[j]			9.9 ± 1.9[j]
			30 ± 5[k]			8 ± 2[k]
Ar^{8+}	16.12	14.9[e]	19 ± 4[k]	6.375	6.2[e]	6.5 ± 2.0[k]

[a]From Froese Fischer and Tachiev [9].
[b]From Curtis *et al.* [89].
[c]From Lawrence and Liszt [91].
[d]From Kernahan *et al.* [92].
[e]From Hibbert *et al.* [8].
[f]From Schlagheck [95].
[g]From Buchet *et al.* [88].
[h]From Kirm *et al.* [90].
[i]From Westerlind *et al.* [22].
[j]From Gardner *et al.* [93].
[k]From Berry *et al.* [94].

and third columns in Table I we compare our calculated and measured values of the excitation energy of $^3P_1$. The rest of the table then compares our predicted and experimental values for the splitting between this $^3P_1$ and the other three levels belonging to $2p^5\,3s$. Starting by comparing our predicted excitation energies of $2p^5\,3s\ ^3P_1$ to experiment, it is found that the difference is largest (0.34%) for neutral neon, while for the rest of the sequence it differs from experiment by less than 0.1%.

The only other level where there are experimental values available all along the sequence is $2p^5\,3s\ ^1P_1$. Again, by comparing our predicted energy splitting between $^3P_1$ and $^1P_1$ to experiment, we find the largest discrepancy for neon, while it decreases rapidly along the isoelectronic sequence and are within 1% from Mg^{2+} up to Ni^{18+}. For higher-Z members, this difference fluctuates as a function of Z. The reason for this is most likely due to large experimental uncertainties for the $^3P_1$ and $^1P_1$ energy splitting, which can be understood from an investigation of the jj-coupling conditions in this part of the isoelectronic sequence. Better notations than $2p^5\,3s\ ^3P_1$ and $^1P_1$ are then $(2p^2_{1/2}\,2p^3_{3/2}\,3s)_1$ and $(2p^1_{1/2}\,2p^4_{3/2}\,3s)_1$, respectively, or $(2p^{-1}_{3/2}\,3s)_1$ and $(2p^{-1}_{1/2}\,3s)_1$, where the superscript -1 represents a hole in the corresponding relativistic subshell. Just as transitions between singlets and triplets are forbidden in an LS-coupled system, a transition of the type $(2p^{-1}_{3/2}\,nl_j)_J - (2p^{-1}_{1/2}\,n'l'_{j'})'_J$ (where $nl \neq n'l'$) is forbidden in a jj-coupled system. If these type of transitions are not found, the energy levels derived from different parent terms, such as $2p^{-1}_{3/2}$ and $2p^{-1}_{1/2}$, are only connected through transitions down to the ground state $2p^6\ ^1S_0$. Since this represents a large gap in energy for Ne-like systems, the uncertainty in experimental energy splitting between levels of the forms $(2p^{-1}_{3/2}\,nl_j)_J$ and $(2p^{-1}_{1/2}\,nl_{j'})_J$ will potentially be large.

Turning to the energy splitting between $^3P_2$ and $^3P_1$, the differences are much smaller and the strong fluctuations found for the splitting to $^1P_1$ for high Z is not found here. This is due to the fact that the these two levels have the same relativistic parent term and will be connected via transitions to common $2p^5\,3p$ levels, leading to smaller experimental uncertainties. Again, our prediction for neutral neon is the most uncertain (1.7% too small), but for the rest of the sequence the agreement between experiment and our theoretical results is well within 1%.

TABLE III. Theoretical $M1$ transition rates (in s^{-1}). Columns 2 to 5 list our results based on different models (see text). The last four columns list results from other theories. The results in the first line for each ion are rescaled to experimental energies, whereas the *ab initio* results are listed in the second row. The "BOE" column contains the "back-of-an-envelope" values calculated as described in Sec. V A. The column labeled "Large" lists values from our large-scale calculation. The notation $x[n] = x \times 10^n$ is used to denote powers of 10.

Ion	LS	jj	BOE	Large	RMBPT-I[a]	RMBPT-II[a]	FAC[a]	MCDHF[b]
Ne	2.517 [−3]	8.389 [−4]	2.303 [−3]	2.310 [−3]				2.334 [−3]
				2.402 [−3]				2.240 [−3]
Na	1.124 [−2]	3.748 [−3]	1.066 [−2]	1.068 [−2]				1.071 [−2]
				1.072 [−2]				1.031 [−2]
Mg	5.164 [−1]	1.721 [−2]	4.864 [−2]	4.871 [−2]				4.880 [−2]
				4.856 [−2]				4.715 [−2]
Al	2.163 [−1]	7.210 [−2]	1.997 [−1]	2.001 [−1]	1.89 [−1]	1.89 [−1]	2.06 [−1]	2.005 [−1]
				1.992 [−1]	3.00 [−1]	4.91 [−5]	1.58 [−1]	1.943 [−1]
Si	8.273 [−1]	2.758 [−1]	7.399 [−1]	7.422 [−1]	7.04 [−1]	7.04 [−1]	7.70 [−1]	7.435 [−1]
				7.374 [−1]	9.94 [−1]	8.49 [−2]	5.97 [−1]	7.223 [−1]
P	2.909[0]	9.696 [−1]	2.490[0]	2.500[0]	2.38[0]	2.38[0]	2.61[0]	2.504[0]
				2.482[0]	3.11[0]	9.12 [−1]	2.05[0]	2.439[0]
S	9.456[0]	3.150[0]	7.658[0]	7.686[0]	7.35[0]	7.34[0]	8.10[0]	7.701[0]
				7.631[0]	9.07[0]	7.57[0]	6.45[0]	7.528[0]
Cl	2.837[1]	9.456[0]	2.156[1]	2.162[1]	2.07[1]	2.08[1]	2.28[1]	
				2.155[1]	2.46[1]	1.74[1]	1.86[1]	
Ar	7.966[1]	2.655[1]	5.645[1]	5.654[1]	5.45[1]	5.45[1]	6.01[1]	
				5.618[1]	6.23[1]	4.83[1]	4.98[1]	
K	2.128[2]	7.092[1]	1.404[2]	1.404[2]	1.36[2]	1.36[2]	1.49[2]	
				1.362[2]	1.48[2]	1.25[2]	1.23[2]	
Ca	5.160[3]	1.720[2]	3.178[2]	3.172[2]	3.09[2]	3.09[2]	3.36[2]	
				3.094[2]	3.30[2]	3.32[2]	2.85[2]	
Sc	1.143[3]	3.811[2]	6.599[2]	6.575[2]	6.43[2]	6.43[2]	6.92[2]	
				6.637[2]	6.98[2]	4.21[2]	6.20[2]	
Ti	2.537[3]	8.455[2]	1.380[3]	1.373[3]	1.35[3]	1.35[3]	1.44[3]	
				1.354[3]	1.41[3]	1.27[3]	1.28[3]	
Cr	9.866[3]	3.289[3]	4.852[3]	4.818[3]	4.76[3]	4.76[3]	4.99[3]	
				4.973[3]	5.11[3]	4.87[3]	4.78[3]	
Fe	3.534[4]	1.178[4]	1.608[4]	1.593[4]	1.58[4]	1.58[4]	1.64[4]	
				1.593[4]	1.62[4]	1.58[4]	1.55[4]	
Ge	7.492[5]	2.497[5]	2.954[5]	2.918[5]	2.91[5]	2.91[5]	2.96[5]	
				2.949[5]	2.97[5]	2.94[5]	2.91[5]	
Br	2.666[6]	8.888[5]	1.010[6]	9.963[5]	9.95[5]	9.95[5]	1.00[6]	
				1.006[6]	1.01[6]	1.00[6]	9.96[5]	

[a]From Beiersdorfer *et al.* [49].
[b]From Fischer and Tachiev [9].

The main focus of this paper is the $^3P_0$ level, with the fewest experimental energy results available. However, it has been experimentally determined for all elements from neutral Ne to Ti^{12+}, together with Cr^{14+}, Fe^{14+}, Ge^{22+}, and Br^{25+}. We agree with experiment well within 1% for all these elements except Ne and Cr^{14+}, where we differ by about 1%. Most interesting to compare with is Fe^{14+}, where the $^3P_1$ - $^3P_0$ magnetic dipole transition has been observed experimentally and the wavelength is determined as 1153.151 ± 0.025 Å [96], in excellent agreement with our predicted value of 1153.150 Å. In Table I experimental energies for more ions are listed, but these are based on interpolation and extrapolation, rather than direct experimental determinations. These cases are marked with an asterisk. In general our predicted energies differ more from these energies than in cases where direct experimental values are available.

To summarize the comparison of our predicted energies with experimental values, it is clear that in most cases we find agreement to a high accuracy, which supports our choice of models. It is also clear that the deviations for the important energy splittings between $^3P_0$ and $^3P_1$ and between $^3P_0$ and $^1P_1$, respectively, are small and will therefore not have a large impact on our predicted hyperfine-induced transition rates.

The hyperfine-induced transition rates are also sensitive to the electric dipole transition matrix elements between $2p^5\,3s\,^3P_1 \rightarrow 2p^6\,^1S_0$ and $2p^5\,3s\,^1P_1 \rightarrow 2p^6\,^1S_0$ and we therefore compare our predicted lifetimes of $2p^5\,3s\,^3P_1$ and $^1P_1$ to experimental and other theoretical [8,9] values in Table II. Unfortunately, as reported in the table, the experimental values all have large errors. Compared with the theoretical predictions in [8] and [9], the overall agreement is good, with the largest differences found at the beginning of the sequence. It is also clear that Hibbert predicts shorter lifetimes than we and Froese Fischer and Tachiev do.

There is one lifetime measurement for the $2p^5\,3s\,^3P_2$ in Fe XVII, by Crespo and Beierdorfer [97], with the result

$4.91^{+0.23}_{-0.08}$ μs, in agreement with our present prediction of 4.84 μs.

A. The $M1$ transition

The $M1$ $2p^5\,3s\,{}^3P_0 \rightarrow 2p^5\,3s\,{}^3P_1$ transition discussed here is a typical example of a forbidden but expected transition and it is therefore arguably straightforward to calculate its rate. This is even more clear since the $M1$ transition operator has, in contrast to other types of transition operators, no radial dependence and the rate therefore only depends on the angular part of the wave functions. When optimizing wave functions to represent different ionic states, only the radial parts of the one-electron wave functions are optimized, whereas the angular parts are assumed to be known. Therefore, to evaluate an $M1$ transition matrix element between two atomic state functions the optimization only contributes through the change in weights c_i of different CSFs in Eq. (17). The $2p^5\,3s\,{}^3P_0 \rightarrow 2p^5\,3s\,{}^3P_1$ $M1$ transition rate can be calculated from [99]

$$\mathcal{A}_{M1} = 2.6973 \times 10^{-11}\sigma^3 \left|\left\langle {}^3P_1 \left|\left|M^{(1)}\right|\right| {}^3P_0 \right\rangle\right|^2, \qquad (20)$$

where

$$M^{(1)} = \sum_i l_i + g_s s_i. \qquad (21)$$

Using LS-coupled CSFs, the $M1$ matrix elements are identical to 0 unless the two CSFs involved have the same configuration, i.e., have the same subshell occupations. In the case of jj coupling, the two CSFs can only differ in the spin coupling of one of the electrons, i.e., for example, $2p_{1/2}$ and $2p_{3/2}$ or $3d_{3/2}$ and $3d_{5/2}$. Since the ASFs of both ${}^3P_1$ and ${}^3P_0$ are completely dominated by the $2p^5\,3s$ configurations, it should be possible to predict the $M1$ rate to a high accuracy taking only these into consideration. According to this, the $M1$ matrix elements for these two CSFs are

$$\left\langle 2p^5\,3s\,{}^3P_1 \left|\left|M^{(1)}\right|\right| 2p^5\,3s\,{}^3P_0 \right\rangle = \sqrt{2}(g_s - 1),$$
$$\left\langle \left(2p_{3/2}^{-1}\,3s\right)_1 \left|\left|M^{(1)}\right|\right| \left(2p_{1/2}^{-1}\,3s\right)_0 \right\rangle = \sqrt{2/3}(g_s - 1),$$
$$\left\langle \left(2p_{1/2}^{-1}\,3s\right)_1 \left|\left|M^{(1)}\right|\right| \left(2p_{1/2}^{-1}\,3s\right)_0 \right\rangle = \sqrt{4/3}(g_s - 1),$$

where $g_s = 2.002\,319\,2$. If experimental energies are available, the $M1$ rate is therefore easy to predict within a factor of 3 since the lowest odd level with $J = 1$ is $2p^5\,3s\,{}^3P_1$ in the case of pure LS coupling and $(2p_{3/2}^{-1}\,3s)_1$ in the case of pure jj coupling. To improve the prediction one can perform a Dirac-Fock calculation to predict the amount of the jj-coupled CSFs $(2p_{3/2}^{-1}\,3s)_1$ and $(2p_{1/2}^{-1}\,3s)_1$ that describes the level that we denote $2p^5\,3s\,{}^3P_1$. These expansion coefficients can then be used together with experimental energies to make a "back of an envelope" (BOE) prediction of the $M1$ rate. These are listed in column 4 in Table III, together with the pure LS- and jj-coupling values in columns 2 and 3.

The $M1$ transition has been investigated by Fischer and Tachiev [9] using the MCHF method and by Beiersdorfer *et al.* [49] using the CI-RMBPT method of FAC [50]. In Table III we compare our results to these earlier calculations for all ions where experimental energies of $2p^5\,3s\,{}^3P_0$ are available. In the fifth column ("Large"), we list the present results from our large-scale calculations. In the last four columns we list earlier predictions from [9] and [49]. For all theoretical results, the second row for each ion lists the *ab initio* results, while the first row lists the rates rescaled to experimental energies.

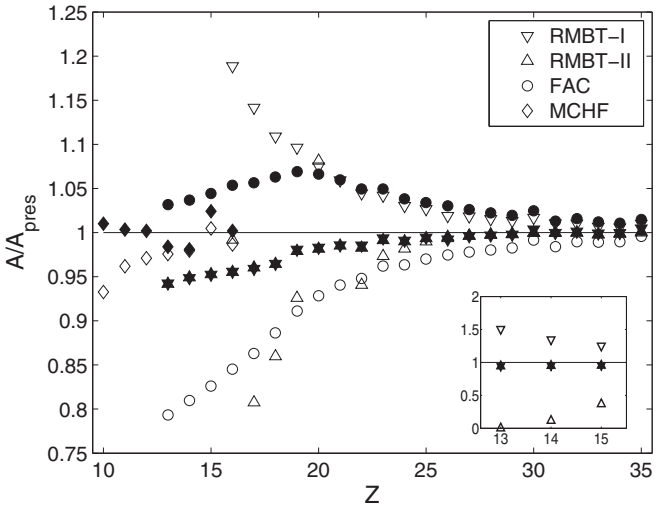

FIG. 2. Different theoretical predictions of the rates for the ${}^3P_0 \rightarrow {}^3P_1$ $M1$ transition in Ne-like ions, relative to our results. Open symbols represent *ab initio* results, while filled symbols represent the rates after rescaling to our transition energies.

We also present a comparison of the different results in Fig. 2. Here, the earlier predictions of Fischer [9] and Beiersdorfer *et al.* [49] are shown relative to our rescaled predictions of the rates. The open symbols represent the *ab initio* results and the filled symbols are the rates rescaled to experimental energies. Note that the rescaled values for RMBT coincide.

We can conclude from Table III that, as expected, the BOE and the "Large" results always fall in the interval between the LS and the jj rates. Comparing the Large and the BOE rates it is found that the differences are very small. Comparing the different $M1$ rates between the different steps in our Large calculations to the final rate, they were found to differ by less than 1% for all ions. Comparing the rescaled $M1$ rates, the differences were even smaller, clearly showing how insensitive this rate is to the accuracy of the representation of the correlation.

Comparing our results to other theoretical work it is clear that both the *ab initio* and the rescaled rates are in very close agreement with the predictions from the MCHF calculations by Fischer and Tachiev [9]. Comparing with the three different calculations by Beiersdorfer *et al.* [49], however, it is found that there are large discrepancies in the lower end of the isoelectronic sequence. To investigate this further, we can note that when the results are rescaled to experimental wavelengths all calculations are in almost-perfect agreement. From the discussion above, it is clear that the expansion coefficients of the $(2p_{3/2}^{-1}\,3s)_1$ and $(2p_{1/2}^{-1}\,3s)_1$ CSFs are the same in the ASF from the RMBPT-I and RMBPT-II calculations, and therefore the transition matrix elements in the two calculations are identical. The differences in the rates are therefore due only to variations in the predicted transition energies. The case of the extremely low transition rate for Al^{3+} predicted by the RMBPT-II method is clearly due only to the fact that

TABLE IV. Hyperfine-induced $2p^6\ ^1S_0$–$2p^5\,3s\ ^3P_0$ electric dipole transition rates, $\mathcal{A}_{\rm HIT}$, compared to the $2p^5\,3s\ ^3P_1$–$2p^5\,3s\ ^3P_0$ magnetic dipole transition rates, $\mathcal{A}_{M1}$ (all in s^{-1}), for stable or long-lived isotopes along the Ne-like isoelectronic sequence ($Z = 10$–35). Also listed are the lifetime (in s) with, τ, and without, τ_{M1}, nuclear spin included, and the branching fraction of the $M1$ transition, Q_{M1}. $x[n] = x \times 10^n$.

Ion	I	μ_I	$\mathcal{A}_{\rm HIT}$	$\mathcal{A}_{M1}$	τ	τ_{M1}	Q_A
^{21}Ne	3/2	−0.661 797	1.3882[0]	2.4016[−3]	7.1911[−1]	4.1638[2]	1.7270[−3]
^{23}Na	3/2	2.217 656	2.6551[1]	1.0718[−2]	3.7648[−2]	9.3301[1]	4.0351[−4]
^{25}Mg	5/2	−0.855 450	6.2049[0]	4.8561[−2]	1.5991[−1]	2.0593[1]	7.7655[−3]
^{26}Al	5	2.804 000	1.0468[2]	1.9915[−1]	9.5348[−3]	5.0213[1]	1.8989[−3]
^{27}Al	5/2	3.641 507	2.0598[2]		4.8502[−3]		9.6591[−4]
^{29}Si	1/2	− 0.555 290	1.8136[1]	7.3740[−1]	5.2985[−2]	1.3561[1]	3.9071[−2]
^{31}P	1/2	1.131 600	1.2833[2]	2.4815[0]	7.6446[−3]	4.0298[−1]	1.8970[−2]
^{33}S	3/2	0.643 821	3.8040[1]	7.6314[0]	2.1896[−2]	1.3104[−1]	1.6709[−1]
^{35}Cl	3/2	0.821 874	9.9200[1]	2.1549[1]	8.2816[−3]	4.6406[−2]	1.7846[−1]
^{36}Cl	2	1.285 470	2.1841[2]		4.1674[−3]		8.9803[−2]
^{37}Cl	3/2	0.684 124	6.8734[1]		1.1076[−2]		2.3868[−1]
^{21}Ar	7/2	− 1.588 000	4.4543[2]	5.6182[1]	1.9936[−3]	1.7799[−2]	1.1200[−1]
^{39}K	3/2	0.391 470	5.3439[1]	1.3619[2]	5.2735[−3]	7.3427[−3]	7.1819[−1]
^{40}K	4	1.298 100	4.4069[2]		1.7335[−3]		2.3608[−1]
^{41}K	3/2	0.214 870	1.6099[1]		6.5665[−3]		8.9429[−1]
^{41}Ca	7/2	− 1.594 781	1.0209[3]	3.0937[2]	7.5173[−4]	3.2324[−3]	2.3256[−1]
^{43}Ca	7/2	− 1.317 643	6.9692[2]		9.9375[−4]		3.0744[−1]
^{45}Sc	7/2	4.756 487	1.3301[4]	6.6369[2]	7.1609[−5]	1.5067[−3]	4.7526[−2]
^{47}Ti	5/2	− 0.788 480	5.7333[2]	1.3543[3]	5.1877[−4]	7.3839[−4]	7.0257[−1]
^{49}Ti	7/2	−1.104170	1.0325[3]		4.1897[−4]		5.6741[−1]
^{50}V	6	3.345 689	1.2210[4]	2.6455[3]	6.7315[−5]	3.7800[−4]	1.7808[−1]
^{51}V	7/2	5.148 706	3.1868[4]		2.8974[−5]		7.6651[−2]
^{21}Cr	3/2	− 0.474 540	4.9131[2]	4.9730[3]	1.8301[−4]	2.0109[−4]	9.1009[−1]
^{51}Mn	5/2	3.568 300	3.2271[4]	9.0365[3]	2.4209[−5]	1.1066[−4]	2.1876[−1]
^{53}Mn	7/2	5.024 000	5.8751[4]		1.4752[−5]		1.3331[−1]
^{55}Mn	5/2	3.468 718	3.0495[4]		2.5296[−5]		2.2859[−1]
^{57}Fe	1/2	0.090 764	6.1188[1]	1.5933[4]	6.2523[−5]	6.2763[−5]	9.9617[−1]
^{59}Co	7/2	4.627 000	9.2257[4]	2.7346[4]	8.3610[−6]	3.6568[−5]	2.2864[−1]
^{61}Ni	3/2	− 0.750 020	4.2145[3]	4.5808[4]	1.9991[−6]	2.1830[−5]	9.1575[−1]
^{63}Cu	3/2	2.227 206	4.9424[4]	7.5066[4]	8.0328[−6]	1.3322[−5]	6.0299[−1]
^{65}Cu	3/2	2.381 700	5.6518[4]		7.5997[−6]		5.7048[−1]
^{67}Zn	5/2	0.875 205	8.4632[3]	1.2057[5]	7.7499[−6]	8.2939[−6]	9.3441[−1]
^{69}Ga	3/2	2.016 590	7.0096[4]	1.9015[5]	3.8425[−6]	5.2590[−6]	7.3065[−1]
^{71}Ga	3/2	2.562 270	1.1316[5]		3.2970[−6]		6.2692[−1]
^{73}Ge	9/2	− 0.879 468	1.2736[4]	2.9487[5]	3.2509[−6]	3.3913[−6]	9.5860[−1]
^{75}As	3/2	1.439 480	6.0239[4]	4.5023[5]	1.9590[−6]	2.2211[−6]	8.8199[−1]
^{77}Se	1/2	0.535 074	1.9298[4]	6.7763[5]	1.4349[−6]	1.4757[−6]	9.7231[−1]
^{79}Se	7/2	− 1.018 000	2.9937[4]		1.4133[−6]		9.5769[−1]
^{79}Br	3/2	2.106 400	2.1305[5]	1.0064[6]	8.2004[−7]	9.9364[−7]	8.2529[−1]
^{81}Br	3/2	2.270 562	2.4755[5]		7.9748[−7]		8.0258[−1]

the predicted energy splitting is 10 times smaller than the experimental value.

A similar problem occurs for the FAC calculations by Beiersdorfer *et al.* [49]. Comparing the *ab initio* results with the rescaled values, it is found that the FAC method predicts too small energy gaps at the beginning of the sequence but the differences are smaller for higher Z's. Comparing the rescaled values to our results it is found that the FAC rates for all ions are higher, by a factor ranging from 3% to 7%. From observations similar to those for the RMBT calculations, it can be concluded that the FAC calculation predicts the system to be more LS-coupled than our calculations, since a more LS-coupled system has smaller energy gaps but a larger transition matrix element.

B. The hyperfine-induced $E1$ transition

The off-diagonal hyperfine interaction opens up an electric dipole transition to the ground state from $2p^5\,3s\ ^3P_0$. This changes both the lifetime of the upper level and the spectra of the ion by redistributing the intensity from the $2p^5\,3s\ ^3P_0 \rightarrow 2p^5\,3s\ ^3P_1$ line to the $2p^5\,3s\ ^3P_0 \rightarrow 2p^6\ ^1S_0$. We list our predicted hyperfine-induced $E1$ transition rates for all stable or long-lived isotopes, with Z ranging from 10 to 35, in Table IV, together with our predicted $M1$ transition rates and lifetimes and the branching fractions of the $M1$ transition.

Since the hyperfine-induced transition rate depends on both the nuclear spin I and the nuclear magnetic dipole moment μ_I it will not show a smooth trend along the isoelectronic

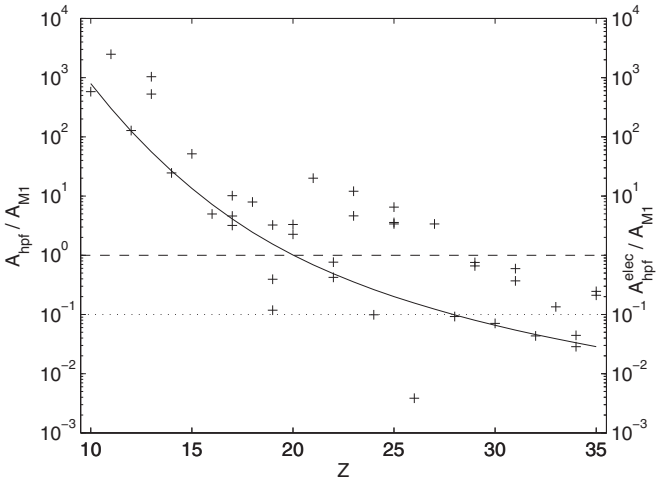

FIG. 3. Ratio between the hyperfine-induced transition and the $M1$ rate along the Ne-like isoelectronic sequence. Crosses correspond to $\mathcal{A}_{\rm HIT}/\mathcal{A}_{M1}$ for different isotopes (scattered due to varying nuclear properties) and the solid line represents the relative value of the electronic part only of the hyperfine-induced transition [as defined in (16)], $\mathcal{A}^{\rm elec}_{\rm HIT}/\mathcal{A}_{M1}$, which should be smooth along the sequence. Dashed and dotted horizontal lines show the 100% and 10% fractions, respectively.

sequence. We therefore plot $A^{\rm elec}_{\rm HIT}$, defined in Eq. (16), relative to A_{M1} along the isoelectronic sequence in Fig. 3 (solid line, right axis). The relative importance of the HIT decreases along the isoelectronic sequence, but at the beginning of the sequence, the hyperfine-induced transition channel clearly dominates in all isotopes with a nuclear spin. As a matter of fact, for all ions investigated here, the hyperfine-induced transition is non-negligible.

Table IV shows that $A_{\rm HIT}$ can be up to three orders of magnitude larger than A_{M1}, therefore drastically shortening the lifetime of the $3s\ ^3P_0$ level. Maybe even more important is that the branching fraction of the $M1$ transition is less than 0.1% in these cases, making the $2p^5\ 3s\ ^3P_0 \rightarrow 2p^5\ 3s\ ^3P_1$ line from these isotopes absent or very weak in spectra of neon-like ions.

VI. CONCLUSION

We have shown the strong impact of the hyperfine-induced transition to the ground state on the decay of the $2p^5\ 3s\ ^3P_0$ level, at the beginning of the Ne-like isoelectronic sequence. This has a strong influence on the spectrum of these ions, even making it isotope dependent. This is also true for the predicted population of this metastable level and, thereby, the predicted ionization distribution of neon in different plasmas. The prediction of the rate of the unexpected HIT, which is induced by the mixing between different atomic states due to interaction with nuclear multipole moments, is a challenge to theory. This is in contrast to the forbidden $M1$ transition to the $2p^5\ 3s\ ^3P_1$ level, which we show is straightforward to predict.

ACKNOWLEDGMENTS

This work was supported by the National Natural Science Foundation of China under Project No. 11074049 and by Shanghai Leading Academic Discipline Project B107. We also gratefully acknowledge support from the Swedish Research Council (Vetenskapsrådet) and the Swedish Institute under the Visby program. J.G. would especially like to thank the Nordic Centre at Fudan University for supporting his exchange visits to Fudan.

[1] W. H. Goldstein, R. S. Walling, J. Bailey, M. H. Chen, R. Fortner, M. Klapisch, T. Phillips, and R. E. Stewart, Phys. Rev. Lett. **58**, 2300 (1987).
[2] S. B. Hansen, A. S. Shlyaptseva, S. A. Pikuz, T. A. Shelkovenko, D. B. Sinars, K. M. Chandler, and D. A. Hammer, Phys. Rev. E **70**, 026402 (2004).
[3] P. Beiersdorfer, S. von Goeler, M. Bitter, and D. B. Thorn, Phys. Rev. A **64**, 032705 (2001).
[4] R. Mewe, A. J. J. Raassen, J. J. Drake, J. S. Kaastra, R. L. J. van der Meer, and D. Porquet, Astron. Astrophys. **368**, 888 (2001).
[5] C. W. Mauche, D. A. Liedahl, and K. B. Fournier, Astrophys. J. **560**, 992 (2001).
[6] U. I. Safronova, M. S. Safronova, and R. Bruch, Phys. Scr. **49**, 446 (1994).
[7] E. P. Ivanova and I. P. Grant, J. Phys. B **31**, 2871 (1998).
[8] A. Hibbert, M. Ledourneuf, and M. Mohan, At. Data Nucl. Data Tables **53**, 23 (1993).
[9] C. Froese Fischer and G. Tachiev, At. Data Nucl. Data Tables **87**, 1 (2004).
[10] E. Avgoustoglou, W. R. Johnson, Z. W. Liu, and J. Sapirstein, Phys. Rev. A **51**, 1196 (1995).
[11] U. I. Safronova, C. Namba, I. Murakami, W. R. Johnson, and M. S. Safronova, Phys. Rev. A **64**, 012507 (2001).
[12] M. J. Vilkas, J. M. López-Encarnación, and Y. Ishikawa, At. Data Nucl. Data Tables **94**, 50 (2008).
[13] I. M. Savukov, W. R. Johnson, and H. G. Berry, Phys. Rev. A **66**, 052501 (2002).
[14] J. Li, T. Brage, P. Jönsson, and Y. Yang, Phys. Rev. A **90**, 035404 (2014).
[15] A. Hibbert and M. P. Scott, J. Phys. B **27**, 1315 (1994).
[16] J. Zeng, G. Dong, G. Zhao, and J. Yuan, J. Phys. B **37**, 2529 (2004).
[17] B. W. Smith, J. B. Mann, R. D. Cowan, and J. C. Raymond, Astrophys. J. **298**, 898 (1985).
[18] H. L. Zhang and D. H. Sampson, At. Data Nucl. Data Tables **43**, 1 (1989).
[19] G.-X. Chen, A. K. Pradhan, and W. Eissner, J. Phys. B **36**, 453 (2003).
[20] S. D. Loch, M. S. Pindzola, C. P. Ballance, and D. C. Griffin, J. Phys. B **39**, 85 (2006).
[21] G.-X. Chen, Phys. Rev. A **76**, 062708 (2007).
[22] M. Westerlind, L. Engström, P. Bengtsson, and L. J. Curtis, Phys. Rev. A **45**, 6198 (1992).

[23] V. Kaufman, M.-C. Artru, and W.-U. L. Brillet, J. Opt. Soc. Am. A **64**, 197 (1974).

[24] H. Gordon, M. G. Hobby, N. J. Peacock, and R. D. Cowan, J. Phys. B **12**, 881 (1979).

[25] C. Jupén, U. Litzén, V. Kaufman, and J. Sugar, Phys. Rev. A **35**, 116 (1987).

[26] P. Beiersdorfer, S. von Goeler, M. Bitter, E. Hinnov, R. Bell, S. Bernabei, J. Felt, K. W. Hill, R. Hulse, J. Stevens, S. Suckewer, J. Timberlake, A. Wouters, M. H. Chen, J. H. Scofield, D. D. Dietrich, M. Gerassimenko, E. Silver, R. S. Walling, and P. L. Hagelstein, Phys. Rev. A **37**, 4153 (1988).

[27] M. F. Gu, P. Beiersdorfer, G. V. Brown, H. Chen, K. R. Boyce, R. L. Kelley, C. A. Kilbourne, F. S. Porter, and S. M. Kahn, Astrophys. J. Lett. **607**, L143 (2004).

[28] J. P. Marques, F. Parente, and P. Indelicato, Phys. Rev. A **47**, 929 (1993).

[29] T. Brage, P. G. Judge, A. Aboussaïd, M. R. Godefroid, P. Jönsson, A. Ynnerman, C. Froese Fischer, and D. S. Leckrone, Astrophys. J. **500**, 507 (1998).

[30] K. T. Cheng, M. H. Chen, and W. R. Johnson, Phys. Rev. A **77**, 052504 (2008).

[31] M. Andersson, Y. Zou, R. Hutton, and T. Brage, Phys. Rev. A **79**, 032501 (2009).

[32] J. P. Marques, F. Parente, and P. Indelicato, At. Data Nucl. Data Tables **55**, 157 (1993).

[33] M. Andersson, Y. Zou, R. Hutton, and T. Brage, J. Phys. B **43**, 095001 (2010).

[34] Y. Liu, R. Hutton, Y. Zou, M. Andersson, and T. Brage, J. Phys. B **39**, 3147 (2006).

[35] T. Brage, P. G. Judge, and C. R. Proffitt, Phys. Rev. Lett. **89**, 281101 (2002).

[36] S. Schippers, E. W. Schmidt, D. Bernhardt, D. Yu, A. Müller, M. Lestinsky, D. A. Orlov, M. Grieser, R. Repnow, and A. Wolf, Phys. Rev. Lett. **98**, 033001 (2007).

[37] S. Schippers, D. Bernhardt, A. Müller, M. Lestinsky, M. Hahn, O. Novotný, D. W. Savin, M. Grieser, C. Krantz, R. Repnow, and A. Wolf, Phys. Rev. A **85**, 012513 (2012).

[38] T. Rosenband, P. O. Schmidt, D. B. Hume, W. M. Itano, T. M. Fortier, J. E. Stalnaker, K. Kim, S. A. Diddams, J. C. J. Koelemeij, J. C. Bergquist, and D. J. Wineland, Phys. Rev. Lett. **98**, 220801 (2007).

[39] K. Yao, M. Andersson, T. Brage, R. Hutton, P. Jönsson, and Y. Zou, Phys. Rev. Lett. **97**, 183001 (2006).

[40] K. Yao, M. Andersson, T. Brage, R. Hutton, P. Jönsson, and Y. Zou, Phys. Rev. Lett. **98**, 269903(E) (2007).

[41] M. Andersson, K. Yao, R. Hutton, Y. Zou, C. Y. Chen, and T. Brage, Phys. Rev. A **77**, 042509 (2008).

[42] M. Andersson, Y. Liu, C. Y. Chen, R. Hutton, Y. Zou, and T. Brage, Phys. Rev. A **78**, 062505 (2008).

[43] W. Du, M. Andersson, K. Yao, T. Brage, R. Hutton, and Y. Zou, J. Phys. B **46**, 145001 (2013).

[44] E. Träbert, P. Beiersdorfer, and G. V. Brown, Phys. Rev. Lett. **98**, 263001 (2007).

[45] S. G. Porsev and A. Derevianko, Phys. Rev. A **69**, 042506 (2004).

[46] M. H. Chen and K. T. Cheng, Can. J. Phys. **89**, 473 (2011).

[47] J. Grumer, T. Brage, M. Andersson, J. Li, P. Jönsson, W. Li, Y. Yang, R. Hutton, and Y. Zou, Phys. Scr. **89**, 114002 (2014).

[48] W. R. Johnson, Can. J. Phys. **89**, 429 (2011).

[49] P. Beiersdorfer, M. Obst, and U. I. Safronova, Phys. Rev. A **83**, 012514 (2011).

[50] M. F. Gu, Can. J. Phys. **86**, 675 (2008).

[51] D. M. Brink and G. R. Satchler, *Angular Momentum* (Clarendon Press, Oxford, UK, 1993).

[52] N. J. Stone, At. Data Nucl. Data Tables **90**, 75 (2005).

[53] I. I. Sobelman, *Atomic Spectra and Radiative Transitions* (Springer-Verlag, Berlin, 1979).

[54] I. P. Grant, *Relativistic Quantum Theory of Atoms and Molecules: Theory and Computation*, Springer Series on Atomic, Optical and Plasma Physics (Springer-Verlag, Berlin, 2007).

[55] P. Jönsson, X. He, C. Froese Fischer, and I. P. Grant, Comput. Phys. Commun. **177**, 597 (2007).

[56] P. Jönsson, G. Gaigalas, J. Bieroń, C. F. Fischer, and I. P. Grant, Comput. Phys. Commun. **184**, 2197 (2013).

[57] I. P. Grant, B. J. McKenzie, P. H. Norrington, D. F. Mayers, and N. C. Pyper, Comput. Phys. Commun. **21**, 207 (1980).

[58] I. P. Grant, J. Phys. B **7**, 1458 (1974).

[59] J. Olsen, M. R. Godefroid, P. Jönsson, P. A. Malmqvist, and C. F. Fischer, Phys. Rev. E **52**, 4499 (1995).

[60] M. Andersson and P. Jönsson, Comput. Phys. Commun. **178**, 156 (2008).

[61] B. O. Roos, P. R. Taylor, and P. E. Siegbahn, Chem. Phys. **48**, 157 (1980).

[62] J. Olsen, B. O. Roos, P. Jorgensen, and H. J. A. Jensen, J. Chem. Phys. **89**, 2185 (1988).

[63] T. Brage and C. F. Fischer, Phys. Scr. **1993**, 18 (1993).

[64] C. Froese Fischer, T. Brage, and P. Jönsson, *Computational Atomic Structure: An MCHF Approach* (Institute of Physics, Bristol, UK, 1997).

[65] D. Layzer, Z. Horák, M. N. Lewis, and D. P. Thompson, Ann. Phys. **29**, 101 (1964).

[66] K. G. Dyall, I. P. Grant, C. T. Johnson, F. A. Parpia, and E. P. Plummer, Comput. Phys. Commun. **55**, 425 (1989).

[67] P. Jönsson, Phys. Scr. **48**, 678 (1993).

[68] I. Lindgren and J. Morrison, *Atomic Many-Body Theory* (Springer-Verlag, Berlin, 1982).

[69] E. B. Saloman and C. J. Sansonetti, J. Phys. Chem. Ref. Data **33**, 1113 (2004).

[70] E. N. Ragozin, S. S. Churilov, E. Y. Kononov, A. N. Ryabtsev, and Y. F. Zayikin, Phys. Scr. **37**, 742 (1988).

[71] J. E. Sansonetti, J. Phys. Chem. Ref. Data **37**, 1659 (2008).

[72] E. Andersson and G.-A. Johannesson, Phys. Scr. **3**, 203 (1971).

[73] J.-P. Buchet, M.-C. Buchet-Poulizac, A. Denis, J. Desesquelles, M. Druetta, S. Martin, J. P. Grandin, X. Husson, and I. Lesteven, Phys. Scr. **31**, 364 (1985).

[74] U. Feldman, G. A. Doschek, and J. F. Seely, Mon. Not. R. Astron. Soc. **212**, 41P (1985).

[75] W. L. Brillet, Phys. Scr. **13**, 289 (1976).

[76] G. Del Zanna and Y. Ishikawa, Astron. Astrophys. **508**, 1517 (2009).

[77] M. Eidelsberg and M.-C. Artru, Phys. Scr. **16**, 109 (1977).

[78] J. Sugar and C. Corliss, J. Phys. Chem. Ref. Data **14**, 1 (1985).

[79] C. Jupén and L. Engström, Phys. Scr. **66**, 140 (2002).

[80] J. P. Buchet, M. C. Buchet-Poulizac, A. Denis, J. Desesquelles, M. Druetta, S. Martin, and J. F. Wyart, J. Phys. B **20**, 1709 (1987).

[81] C. Jupén, Phys. Scr. **36**, 776 (1987).

[82] G. Yuan, Y. Kato, H. Daido, R. Kodama, K. Murai, and T. Kagawa, Phys. Scr. **53**, 197 (1996).
[83] L. Engström and H. G. Berry, Phys. Scr. **34**, 131 (1986).
[84] C. Jup'en, I. Martinson, X. T. Zeng, S. B. Du, J. W. Li, L. Y. Jiang, H. Z. Chen, H. W. Yu, Y. M. Li, and Y. B. Qiu, Phys. Scr. **61**, 443 (2000).
[85] J. E. Sansonetti, J. Phys. Chem. Ref. Data **37**, 7 (2008).
[86] A. Kramida, Yu. Ralchenko, J. Reader, and NIST ASD Team, *NIST Atomic Spectra Database (version 5.2)* (National Institute of Standards and Technology, Gaithersburg, MD, 2015).
[87] C. Jup'en, U. Litz'en, and B. Skogvall, Phys. Scr. **33**, 69 (1986).
[88] J. P. Buchet, M. C. Buchet-Poulizac, and P. Ceyzeriat, Phys. Lett. A **77**, 424 (1980).
[89] L. J. Curtis, S. T. Maniak, R. W. Ghrist, R. E. Irving, D. G. Ellis, M. Henderson, M. H. Kacher, E. Träbert, J. Granzow, P. Bengtsson, and L. Engström, Phys. Rev. A **51**, 4575 (1995).
[90] M. Kirm, P. Bengtsson, and L. Engström, Phys. Scr. **54**, 167 (1996).
[91] G. M. Lawrence and H. S. Liszt, Phys. Rev. **178**, 122 (1969).
[92] J. A. Kernahan, A. Denis, and R. Drouin, Phys. Scr. **4**, 49 (1971).
[93] R. K. Gardner, C. L. Cocke, T. K. Saylor, and B. Curnutte, J. Opt. Soc. Am. **68**, 830 (1978).
[94] H. G. Berry, J. Desesquelles, K. T. Cheng, and R. M. Schectman, Phys. Rev. A **18**, 546 (1978).
[95] W. Schlagheck, Phys. Lett. A **54**, 181 (1975).
[96] U. Feldman, W. Curdt, E. Landi, and K. Wilhelm, Astrophys. J. **544**, 508 (2000).
[97] J. R. C. L'opez-Urrutia and P. Beiersdorfer, Astrophys. J. **721**, 576 (2010).
[98] T. Brage, M. Andersson, and R. Hutton, in *American Institute of Physics Conference Series*, edited by S. Zhu and J. Yan (American Institute of Physics, Melville, NY, 2009), Vol. 1125, pp. 18–28.
[99] R. D. Cowan, *The Theory of Atomic Structure and Spectra* (University of California Press, Berkeley, 1981).